Investigating Voltage Excitation of the Darwin Model via the Prescription of Terminal Scalar Potentials

K. Roppert, S. Kvasnicka, C. Riener, T. Bauernfeind, and M. Kaltenbacher

Institute of Fundamentals and Theory in Electrical Engineering, Graz University of Technology, 8010 Graz, Austria
TU-Graz SAL GEMC Lab, Silicon Austria Labs, 8010 Graz, Austria

Developing simulation models for electromagnetic field problems often deals with approximations of the full set of Maxwell's equations, to obtain performant methods. This is also the case for the so-called Darwin model, which has the capability of including resistive, inductive, and capacitive effects without the need of solving full-wave Maxwell's equations. However, an issue is the difficulty of prescribing realistic excitations of the model, e.g., via a terminal voltage. In this article, the straightforward prescription of the scalar potential on electric ports is investigated via Poynting's theorem, with the outcome that it can be considered as physical voltage excitation up to frequencies, where the validity of the Darwin model itself is lost.

***Index Terms*— Computational electromagnetics, Darwin model, finite element (FE) analysis, Maxwell equations, numerical simulation.**

I. Introduction

THE Darwin approximation of Maxwell's equations is of great theoretical and practical importance because it includes resistive, inductive, and capacitive effects, without the need for solving a hyperbolic wave equation in the time domain, respectively, the full set of Maxwell's equations. This model, described in Section II, is a quasi-stationary approximation of the full set of Maxwell's equations, neglecting wave phenomena, and therefore, it is only valid up to frequencies, where wave effects start to become dominant [1]

$$f \ll f_{\max} = \frac{c_{\min}}{d} = \frac{c_0}{d \cdot \sqrt{\mu_{r,\max} \cdot \varepsilon_{r,\max}}}$$

where c_0 is the speed of light in vacuum, d is the spatial expansion of the application (characteristic length), and $\mu_{r,\max}$ and $\varepsilon_{r,\max}$ are the maximum relative magnetic permeability and electric permittivity, respectively.

An important step toward a practically feasible method is the physically correct excitation of the model. The interpretation of a voltage excitation via electric ports at the surface of the computational domain is more involved as for the classical eddy current problem, because (Darwin-) displacement currents have to be taken into consideration too.

In the following, the proposed formulation in the frequency domain of the Darwin model is presented in Section II based on [2], which is an explicitly gauged formulation using the generalized Coulomb gauge and it results in a symmetric formulation. Together with this formulation and Poynting's theorem, the issue regarding the terminal voltage excitation of the Darwin model is shown in Section III, where special attention is paid to make plausible and physically sound assumptions on the currents at the electric ports. In Section IV, the physical voltage excitation via potential at the electric ports, investigated in Section III, is applied to a finite element (FE) implementation of the Darwin approximation in openCFS [5] on two examples, a simple parallel plate capacitor and a capacitor in series with a copper coil. The Darwin results are then critically compared with full-wave solution, simulated with SIMULIA CST Studio Suite.

Manuscript received 10 February 2022; revised 20 March 2022; accepted 23 May 2022. Date of publication 26 May 2022; date of current version 26 August 2022. Corresponding author: K. Roppert (e-mail: klaus.roppert@tugraz.at).

Color versions of one or more figures in this article are available at https://doi.org/10.1109/TMAG.2022.3178139.

Digital Object Identifier 10.1109/TMAG.2022.3178139

II. $(\mathbf{A}, \varphi, p)$ Formulation of the Darwin Model

The Darwin model is an approximation to the full set of Maxwell's equations, by neglecting the second time derivative of the magnetic vector potential $\partial_t \partial_t \boldsymbol{A} = \mathbf{0} \hat{=} -\omega^2 \hat{\boldsymbol{A}} = \mathbf{0}$.

The use of a scalar potential $\hat{\varphi}$ and the magnetic vector potential $\hat{\boldsymbol{A}}$, as well as the relationships $\hat{\boldsymbol{E}} = -\nabla\hat{\varphi} - j\omega\hat{\boldsymbol{A}}$ and $\hat{\boldsymbol{B}} = \operatorname{curl}\hat{\boldsymbol{A}}$, leads to the following $(\boldsymbol{A}, \varphi)$ formulation in the frequency domain

$$\operatorname{curl}\left(\mu^{-1}\operatorname{curl}\hat{\boldsymbol{A}}\right) + j\omega\gamma\,\hat{\boldsymbol{A}} + \gamma\,\nabla\hat{\varphi} + j\omega\varepsilon\,\nabla\hat{\varphi} = \hat{\boldsymbol{J}}_i \quad (1a)$$

$$-\operatorname{div}\left(j\omega\gamma\,\hat{\boldsymbol{A}}\right) - \operatorname{div}\left(\gamma\,\nabla\hat{\varphi}\right) - \operatorname{div}\left(j\omega\varepsilon\nabla\hat{\varphi}\right) = 0 \quad (1b)$$

where γ is the electric conductivity, ω is the angular velocity, μ is the magnetic permeability, and ε is the permittivity. Equation (1a) corresponds to the approximated Ampère–Maxwell equation, which takes only an irrotational part of the displacement current into account and (1b) corresponds to the approximated continuity law.

In order to overcome the difficulty of an ill-conditioned and nonsymmetric system, which (1a) and (1b) lead to, Zhao and Tang [2] proposed an improved formulation by introducing a Lagrange multiplier p and an additional constraint to ensure that $j\omega\hat{\boldsymbol{A}}$ is ε-divergence-free. This leads to the following formulation in the frequency domain:

$$\begin{aligned}
&\operatorname{curl}\left(\mu^{-1}\operatorname{curl}\hat{\boldsymbol{A}}\right) + \gamma\,\left(j\omega\hat{\boldsymbol{A}} + \nabla\hat{\varphi}\right) + j\omega\varepsilon\,\nabla\hat{\varphi} \\
&\quad - j\omega\varepsilon\,\nabla p = \hat{\boldsymbol{J}}_i \\
&\frac{1}{j\omega}\operatorname{div}\Big(-\gamma\,\left(j\omega\hat{\boldsymbol{A}} + \nabla\hat{\varphi}\right) - j\omega\varepsilon\,\nabla\hat{\varphi}\Big) - \operatorname{div}\left(j\omega\varepsilon\,\hat{\boldsymbol{A}}\right) = 0 \\
&\operatorname{div}\left(j\omega\varepsilon\,\hat{\boldsymbol{A}}\right) = 0. \qquad (2)
\end{aligned}$$

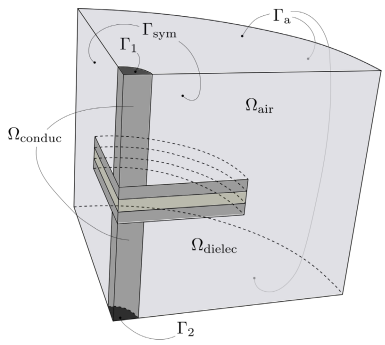

Fig. 1. Computational domain (quarter model).

This approach implies a symmetric complex matrix system after FE discretization; see [2] and [3] for further details. In the following, the impressed current density $\hat{\boldsymbol{J}}_i$ is neglected in favor of a more concise notation.

III. Voltage Excitation

In the classical ($\boldsymbol{A} - V$) formulation of the eddy current problem, the voltage between two electric ports can easily be interpreted as the difference in the electric scalar potential V and by prescribing V at the ports, and voltage excitation can be realized. When using the Darwin approximation, this interpretation must be investigated, which will be discussed in the following. Contrary to the formulation in (2), the following derivation is written in the time domain, due to a more concise notation; however, it holds true also for the complex case in the frequency domain.

Let us consider the computational domain, depicted in Fig. 1. The goal is to investigate the physical interpretation of prescribing the scalar potential φ at the electric ports Γ_1 and Γ_2 as a Dirichlet boundary condition (BC). The remaining BCs for $\boldsymbol{A}$, φ, and p are chosen as: $\mathrm{tr}_\tau(\boldsymbol{A}) = 0$ on $\partial\Omega$, natural BCs for φ on $\partial\Omega \setminus \{\Gamma_1 \cup \Gamma_2\}$, $p = 0$ on $\partial\Omega \setminus \Gamma_{\mathrm{sym}}$, and natural BCs for p on Γ_{sym}. The port BCs on Γ_1 and Γ_2 on the boundary of the computational domain can then be physically interpreted as electric circuit element BCs.

Since the electric field is not conservative, the definition of a voltage $u = \int_{\mathcal{C}} \boldsymbol{E} \cdot \boldsymbol{\tau}$ depends on the curve $\mathcal{C}$ and is not feasible to describe voltage excitation. If, however, the voltage is defined via the power $P = u\,i$, Poynting's theorem can be used to identify what the prescription of a scalar potential φ on the electric ports implies, following the idea from [6]. Let us recall Poynting's theorem on the whole computational domain Ω and bounding surface $\partial\Omega$ as

$$(\boldsymbol{H}, \partial_t \boldsymbol{B})_\Omega + (\boldsymbol{E}, \partial_t \boldsymbol{D})_\Omega + (\boldsymbol{E}, \boldsymbol{J})_\Omega = -\langle \boldsymbol{E} \times \boldsymbol{H}, \boldsymbol{n} \rangle_{\partial\Omega} = P \tag{3}$$

where $\boldsymbol{n}$ is the outer normal to $\partial\Omega$ as well as $(\cdot,\cdot)_\Omega$ and $\langle \cdot,\cdot \rangle_{\partial\Omega}$ denotes a volume and surface integral with a dot product between both arguments, respectively. Furthermore, ∂_t denotes the time derivative operator and P the change in inner energy per unit time.

Poynting's theorem implies that the energy state of the system can be changed by either boundary or volumetric power sources. Inserting approximated Darwin–Ampère and Faraday's law as well as the two potentials $\boldsymbol{A}$ and φ and using Green's identities, (3) takes the form

$$-\langle \varphi \boldsymbol{J}, \boldsymbol{n} \rangle_{\partial\Omega} - \langle \varphi\, \varepsilon\, \partial_t \nabla\varphi, \boldsymbol{n} \rangle_{\partial\Omega} = P. \tag{4}$$

Due to $\boldsymbol{J} = \gamma\, \boldsymbol{E}$ and the fact that the only conducting parts at the boundary of the whole computational domain Ω are the electric ports Γ_1 and Γ_2, both surface integrals reduce to the surface of the electric ports, because $\nabla\varphi \cdot \boldsymbol{n} = 0$ and $\gamma = 0$ on $\partial\Omega \backslash \{\Gamma_1 \cup \Gamma_2\}$.

Assuming the prescription of spatial independent scalar potential at the ports $\varphi_{|\Gamma_k} = \varphi_k$ for $k \in \{1, 2\}$, it further reduces to

$$\begin{aligned} &-\varphi_1 \underbrace{\langle \boldsymbol{J}, \boldsymbol{n} \rangle_{\Gamma_1}}_{\text{current } i_c} - \varphi_2 \underbrace{\langle \boldsymbol{J}, \boldsymbol{n} \rangle_{\Gamma_2}}_{-i_c} - \sum_{k=1}^{2} \langle \varphi\, \varepsilon\, \partial_t \nabla\varphi, \boldsymbol{n} \rangle_{\Gamma_k} \\ &= (\varphi_2 - \varphi_1)\, i_c - \varphi_1 \underbrace{\langle \varepsilon\, \partial_t \nabla\varphi, \boldsymbol{n} \rangle_{\Gamma_1}}_{\text{displacement current } i_d} - \varphi_2 \underbrace{\langle \varepsilon\, \partial_t \nabla\varphi, \boldsymbol{n} \rangle_{\Gamma_2}}_{-i_d} \\ &= (\varphi_2 - \varphi_1)\, (i_c + i_d) = (\varphi_2 - \varphi_1), \quad i = u,\ i = P \end{aligned} \tag{5}$$

from which the current i_c via the transport of free electric charges and the Darwin-displacement current i_d can be identified, whereas in the classical eddy current case, only i_c can occur.

However, this straightforward evaluation of (4) implicitly makes the assumption that the ratios of conducting currents and displacement currents are the same at the electric ports

$$\begin{aligned} \langle \boldsymbol{J}, \boldsymbol{n} \rangle_{\Gamma_2} &= -\langle \boldsymbol{J}, \boldsymbol{n} \rangle_{\Gamma_1} \\ \langle \varepsilon\, \partial_t \nabla\varphi, \boldsymbol{n} \rangle_{\Gamma_2} &= -\langle \varepsilon\, \partial_t \nabla\varphi, \boldsymbol{n} \rangle_{\Gamma_1} \end{aligned} \tag{6}$$

which cannot be conclusively justified from a physical point of view. This issue can be solved by making mathematically rigorous and plausible assumptions on the whole computational domain Ω and its boundary $\partial\Omega$, which fulfill the preconditions of a weak divergence theorem, e.g., according to [4]. To fulfill the conditions for this theorem (sometimes also referred to as weak Gauß theorem), the domain must be $\Omega \subseteq \mathbb{R}^n$ (used here for $n = 3$) open and bounded with a Lipschitz boundary, which is the case for all the domains that are used in this work (not necessarily C^1 but definitely Lipschitz). This now allows to describe the relationship between the port currents $i_{\Gamma_k} = \langle \boldsymbol{J} + \varepsilon\, \partial_t \nabla\varphi, \boldsymbol{n} \rangle_{\Gamma_k}$ as follows, using the Darwin approximated continuity law (1b):

$$\begin{aligned} 0 &= \int_\Omega \mathrm{div}\left(\boldsymbol{J} + \varepsilon \partial_t \nabla\varphi\right) = \langle \boldsymbol{J} + \varepsilon\, \partial_t \nabla\varphi, \boldsymbol{n} \rangle_{\partial\Omega} \\ &= i_{\Gamma_1} + i_{\Gamma_2}. \end{aligned} \tag{7}$$

Applying this result on (4) leads to

$$-\varphi_1\, i_{\Gamma_1} - \varphi_2\, i_{\Gamma_2} = (\varphi_2 - \varphi_1)\, i_{\Gamma_1} = u\, i = P. \tag{8}$$

Here, $i_{\Gamma_k} = i_{c_k} + i_{d_k}$ contains the current $i_{c_k} = \langle \boldsymbol{J}, \boldsymbol{n} \rangle_{\Gamma_k}$ resulting from the transport of free electric charges and the Darwin-displacement current $i_{d_k} = \langle \varepsilon\, \partial_t \nabla\varphi, \boldsymbol{n} \rangle_{\Gamma_k}$. This result looks very similar to the one in (5) but with the major difference that the ratios of conducting currents and Darwin-displacement currents do not need to be identical on

both electric ports. To conclude, it can be stated that the prescription of electrical scalar potentials at the ports corresponds to an actual physical voltage excitation.

However, there are frequency-dependent differences in the order of magnitude between the conducting current and Darwin-displacement current. For low frequencies, the time derivative multiplied with the, for practical applications, very small electric permittivity ε results in a negligible Darwin-displacement current i_{d_k} term, compared with the conducting currents i_{c_k}, and approximately, only resistive and inductive effects are present. Increasing the frequency such that the latter becomes dominant, an additional capacitive behavior and non-zero displacement currents occur, which are clearly visible in the frequency analysis of the numerical examples (see Figs. 3 and 6).

IV. Numerical Verification

A. Parallel Plate Capacitor

In the first example, a parallel plate capacitor with a dielectric material between its plates is considered, as depicted in Fig. 1. The diameter of the feed lines and capacitor plates is $d_{\text{feed}} = 0.5$ mm and $d_{\text{plate}} = 12$ mm, respectively, both made of copper with an electric conductivity of $5.7 \cdot 10^7$ Sm^{-1}. Both the feed lines have a length of $l_{\text{feed}} = 5$ mm, and the height of the dielectric is $h_{\text{dielec}} = 1$ mm with $\varepsilon_r = 10000$. This leads to an analytic approximation of the capacity for low frequencies $C_a = \varepsilon_r \varepsilon_0 \pi (d_{\text{plate}}/2)^2 / h_{\text{dielec}} = 10.0139$ nF, which will be used later on as a reference for impedance in the low-frequency region.

The aim of this example is first to verify the implemented Darwin model in the frequency domain with a full-wave solution and second to test the postulated voltage excitation of the Darwin model from Section III. For this purpose, the full-wave solution using CST Studio Suite was used as a reference with the same geometrical dimensions, mesh resolution, and solution domain as for the Darwin model, including a mesh refinement in the conducting regions to resolve the skin penetration depth with approximately five elements. A current excitation via the electrical ports Γ_1 and Γ_2 was specified in CST, and the complex impedance was evaluated at different frequencies, which was compared with the results from the Darwin model with a prescription of $\varphi_1(t) = 1\ \text{V} \sin(\omega t)$ and $\varphi_2(t) = 0$ V. To evaluate the impedance of the Darwin model, the surface integral of the total current was computed as

$$\hat{i}_{\text{total}} = \int_{\Gamma_1} \left(\gamma\, \hat{\boldsymbol{E}} + j\omega\varepsilon \hat{\boldsymbol{D}}\right) \cdot \boldsymbol{n} \tag{9}$$

where the notation $\hat{(\cdot)}$ is used to denote a complex quantity from a harmonic simulation. Inserting the magnetic vector potential $\hat{\boldsymbol{A}}$, the scalar potential $\hat{\varphi}$, and the Darwin approximation $\partial_t \partial_t \boldsymbol{A} \hat{=} -\omega^2 \hat{\boldsymbol{A}} = 0$, we arrive at the (Darwin-) approximated total current $\hat{\tilde{i}}_{\text{total}}$ through the electric port

$$\hat{i}_{\text{total}} \approx \hat{\tilde{i}}_{\text{total}} = \int_{\Gamma_1} \left(-\gamma \left(\nabla\hat{\varphi} + j\omega\hat{\boldsymbol{A}}\right) + j\omega\varepsilon\nabla\hat{\varphi}\right) \cdot \boldsymbol{n}. \tag{10}$$

In Fig. 2, the comparison between the absolute value of impedance computed via the Darwin total current according to (10) and the full-wave current $\hat{i}_{\text{total}}$ from (9) is displayed. Furthermore, an estimate can be given according to [1] for the maximum frequency $f_{\max}$ which indicates that for $f \geq f_{\max}$, wave phenomena are dominant and cannot be neglected. This frequency threshold can also be considered as an upper bound for the frequency range in which the Darwin model itself can provide valid results. A common rule of thumb is that for the conservative estimation $f \leq f_{\max}/10$, wave effects can be neglected. However, since the Darwin model incorporates a part of the displacement current, Fig. 2 also shows satisfying results for $f_{\max}/10 < f < f_{\max}$. Furthermore, the frequency dependency of the conducting and Darwin-displacement currents is depicted in Fig. 3. This clearly shows that the displacement currents, more precisely the Darwin-displacement currents, become more dominant and significant for increasing frequencies, as described in Section III.

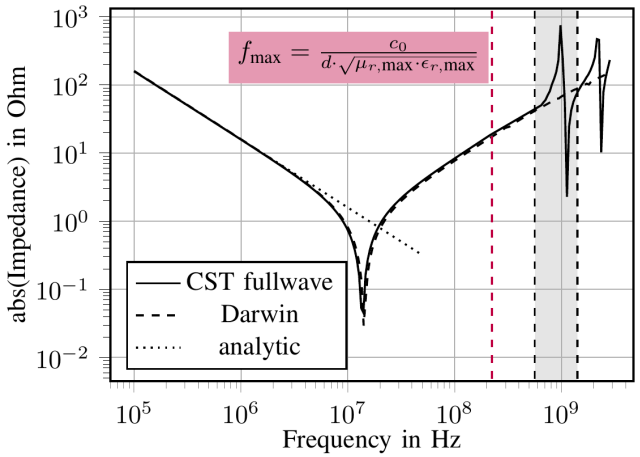

Fig. 2. Comparison of absolute value of the impedance for the Darwin model with full-wave results, evaluated for the plate capacitor. The shaded region depicts an unphysical domain resonance due to $\boldsymbol{n} \times \boldsymbol{E} = \boldsymbol{0}$ BCs in CST.

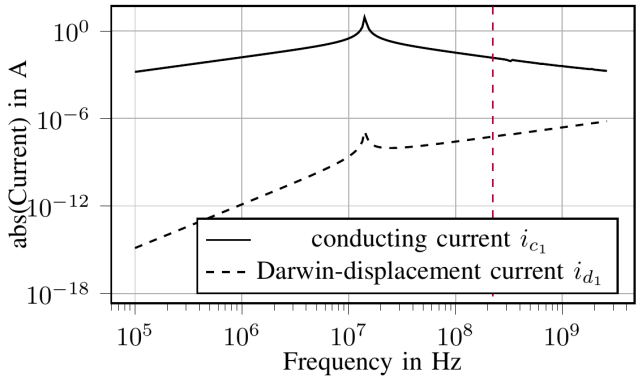

Fig. 3. Depiction of the different current components for the parallel plate capacitor setup, simulated with the Darwin model. The red dashed line depicts the same maximum frequency limit as in Fig. 2.

B. Capacitor With Coil

In the second example, the parallel plate capacitor from Section IV-A is connected to an air coil in series, in accordance with Fig. 4, embedded in an air domain. However, in contrast to Section IV-A, in this example $\varepsilon_r = 1000$ is used, which leads to an analytic approximation of the capacity for low frequencies $C_a = \varepsilon_r \varepsilon_0 \pi (d_{\text{plate}}/2)^2 / h_{\text{dielec}} = 1.00139$ nF.

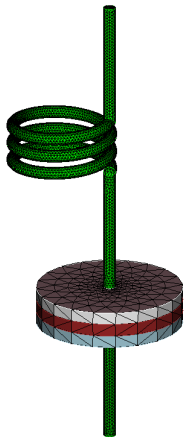

Fig. 4. Model of a common series resonant circuit, embedded in an air domain, which is not depicted due to better visibility.

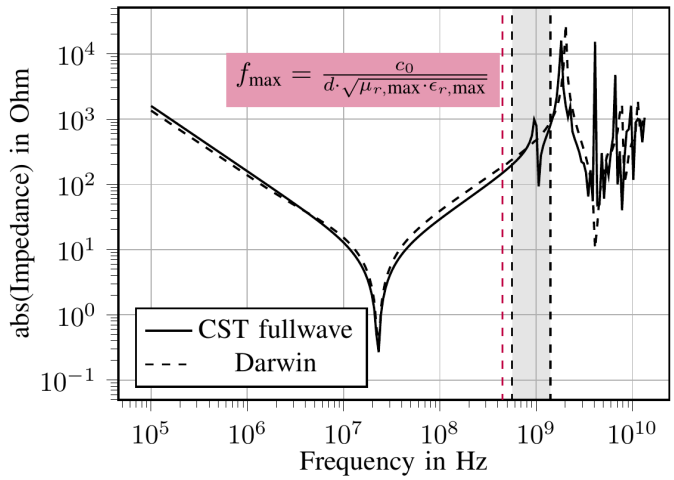

Fig. 5. Comparison of absolute value of the impedance for the Darwin model with full-wave results, evaluated for the series resonant circuit according to Fig. 4. The shaded region depicts an unphysical domain resonance due to $\boldsymbol{n} \times \boldsymbol{E} = \boldsymbol{0}$ BCs in CST.

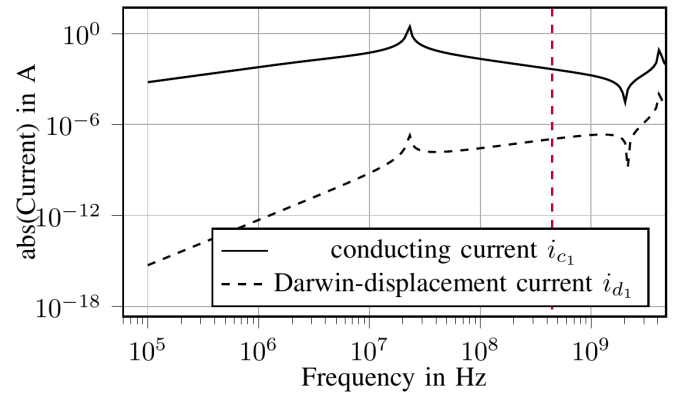

Fig. 6. Depiction of different current components for the capacitor with coil setup, simulated with the Darwin model. The red dashed line depicts the same maximum frequency limit as in Fig. 5.

Similarly as described in Section IV-A, the total current $\hat{i}_{\text{total}}$ and (Darwin-) approximated total current $\hat{\tilde{i}}_{\text{total}}$ are evaluated, according to (9) and (10), respectively. Fig. 5 depicts the comparison of impedance using voltage excitation with $\varphi_1(t) = 1\ \text{V}\sin(\omega t)$ and $\varphi_2(t) = 0\ \text{V}$ and the evaluated currents $\hat{i}_{\text{total}}$ and $\hat{\tilde{i}}_{\text{total}}$, respectively. Here, Fig. 5 shows good concordance of the absolute value of impedance for $f \leq f_{\max}/10$ and a small deviation in the frequency range $f_{\max}/10 < f < f_{\max}$. Therefore, it must be noted that CST simulation uses current excitation and imposes BCs $\boldsymbol{n} \times \boldsymbol{E} = \boldsymbol{0}$, and on the other hand, the Darwin model uses voltage excitation and BCs as described in Section III. Nevertheless, the Darwin model leads to meaningful results up to $f_{\max}$ and also the frequency behavior of the total current parts (conducting and Darwin-displacement currents) as described in Section III can be observed in Fig. 6.

V. Conclusion

A physically correct and realistic excitation is important for applications of all types of Maxwell's equations. In this work, it was rigorously shown that the prescription of terminal scalar potentials in the Darwin model can in fact be considered as physical voltage excitation under certain assumptions regarding the computational domain. At this point, it is important to mention that the derivation in Section III, using Poynting's theorem, only works for domains, where the electric ports Γ_1 and Γ_2 are located at the outer boundary of the global domain ($\Gamma_1 \cup \Gamma_2 \subseteq \partial\Omega$) and that the boundary of the domain is a Lipschitz boundary. As stated in Section I, the Darwin model is valid up to frequencies where wave effects become dominant, which was also shown in both numerical examples in Section IV. This is also the frequency range, where the potential difference at the electric ports can be interpreted as a physical voltage.

In future work, this derivation should be carried out for more than two electric ports and for a total current excitation, which is sometimes more practically relevant, especially if results are compared with measurements later on.

Acknowledgment

This work was supported by "University SAL Labs" Initiative of Silicon Austria Labs (SAL) and its Austrian Partner Universities for Applied Fundamental Research for Electronic-Based Systems.

The authors thank Dassault Systèmes Simulia Corporation, Johnston, RI USA, for providing them their software SIMULIA CST Studio Suite.

References

[1] S. Koch and T. Weiland, "Different types of quasi-stationary formulations for time domain simulations," *Radio Sci.*, vol. 46, no. 5, pp. 1–7, 2011.

[2] Y. Zhao and Z. Tang, "A novel gauged potential formulation for 3-D electromagnetic field analysis including both inductive and capacitive effects," *IEEE Trans. Magn.*, vol. 55, no. 6, pp. 1–5, Jun. 2019.

[3] S. Yan, Z. Tang, T. Henneron, and Z. Ren, "Structure-preserved reduced-order modeling for frequency-domain solution of the Darwin model with a gauged potential formulation," *IEEE Trans. Magn.*, vol. 56, no. 1, pp. 1–4, Jan. 2020.

[4] H. W. Alt and R. Nürnberg, *Linear Functional Analysis: An Application-Oriented Introduction*. London, U.K.: Springer, 2016.

[5] M. Kaltenbacher, *Numerical Simulation of Mechatronic Sensors and Actuators: Finite Elements for Computational Multiphysics*. Cham, Switzerland: Springer, 2015.

[6] R. Hiptmair and O. Sterz, "Current and voltage excitations for the eddy current model," *Int. J. Numer. Model., Electron. Netw., Devices Fields*, vol. 18, no. 1, pp. 1–21, Jan. 2005.